Preparation of konjac glucomannan based films reinforced with nanoparticles and its effect on cherry tomatoes preservation

Fei Xiang[a,b], Yuting Xia[a,b], Yan Wang[a,b], Yixin Wang[c], Kao Wu[a,b], Xuewen Ni[a,b,*]

[a]Glyn O. Philips Hydrocolloid Research Centre at HUT, Hubei University of Technology, Wuhan 430068, China

[b]School of Bioengineering and Food Science, Hubei University of Technology, Wuhan 430068, China

[c]Faculty of Engineering, University of Nottingham, University Park, Nottingham, NG72RD, UK

*Corresponding author at: Glyn O. Philips Hydrocolloid Research Centre at HUT, Hubei University of Technology, Wuhan 430068, China

E-mail address: nixuewen@126.com (X. Ni).

Abstract

Present study aims to investigate the effect of nanoparticles (zein nanoparticles, nanocellulose, nano-TiO_2, nano-SiO_2) incorporation on rheological properties of film-forming solutions and physicochemical properties of konjac glucomannan (KGM) based films, and to evaluate the effect of KGM/nanoparticles blend film on cherry tomatoes preservation. The results showed that the blend film-forming solutions exhibited shear-thinning behavior, and KGM/zein nanoparticle film-forming solution showed the lowest crossover frequency value of storage (G′) and loss (G") moduli due to enhanced molecular interaction and entanglement. The nanoparticles were dispersed homogeneously in the KGM continuous matrix and had good compatibility with KGM, thereby improving physicochemical properties of KGM based films. KGM/zein nanoparticle blend film (KNZ) showed the best properties, such as smoother surface and denser cross-section, the highest glass transition temperature and elongation at break, as well as the best moisture and oxygen barrier. In comparison with the control and polyethylene film packaging, cherry tomatoes in KNZ film packaging showed lower weight loss and firmness reduction, and had relatively stable content of total soluble solids, vitamin C content and pH value during storage up to 10 days at 26 °C. The results suggested the high potential of KNZ film for application in cherry tomatoes preservation.

Keywords: rheology; microstructure; physical properties; preservation

1. Introduction

Traditional plastic packaging is a non-degradable deadly pollutant that will cause environmental degradation. Degradable packaging made from natural polymers is considered a viable alternative to conventional plastic packaging (Castro-Rosas et al., 2016). Natural polymers such as proteins, polysaccharides and lipids are renewable resources, which can be used as structural matrices to prepare degradable packaging. Konjac glucomannan (KGM) is a kind of water-soluble high molecular weight neutral polysaccharide extracted from the tubers of *Amorphophallus konjac* C. Koch. It is mainly composed of glucose and mannose residues (1:1.6) polymerized through β-1,4 glycosidic bonds (Yoshimura, & Nishinari, 1999; Kato, & Matsuda, 1969). KGM has a good film-forming performance and is a promising raw material for making degradable packaging (Ni et al., 2018; Li et al., 2015). However, pure KGM film has the defects of poor water resistance and low mechanical strength, which limit its application in biodegradable packaging (Wang et al., 2017). For these reasons, research efforts have been focused on the property modification of KGM based films. KGM was frequently blended with other natural polymers to enhance these features, e.g. with curdlan (Wu et al., 2012), starch (Chen et al., 2008), whey protein isolate (Leuangsukrerk et al., 2014) and gelatin (Xiao, Lu, Gao, & Zhang, 2001). Our group found that the blend films made of KGM and hydrophobic zein or ethyl cellulose exhibited increased thermal stability, mechanical properties and water resistance (Wang et al., 2017; Li et al., 2015).

In recent years, the application of nanoparticles in the packaging industry has attracted attention. These particles are of importance because of their small size, high surface energy and large specific surface area. Nanoparticles are used as reinforcement materials in biodegradable films to improve their functional properties (mechanical, barrier, etc.), and polymer nanocomposites exhibit the large-scale improvement in the physicochemical properties compared with conventional composites (Rhim, & Ng, 2007; Azeredo, Rosa, & Mattoso, 2017). The development of polymer nanocomposites promises to expand the use of biodegradable films. As reported, nano-SiO_2 (NS) could significantly improve the water resistance, light transmission and mechanical properties of the starch/polyvinyl alcohol (PVA) film due to the good miscibility, an intermolecular hydrogen bond and a strong chemical bond C-O-Si between the NS and starch/PVA (Tang, Xiong, Tang, & Zou, 2009). Zein nanoparticles (NZ) have the characteristics of natural origin, mild preparation conditions, high probability of industrial production, good biocompatibility and strong affinity to bioactives (Li, Wang, Liu et al., 2019). Zhang and Zhao (2017) reported that the incorporation of zein-rutin composite nanoparticles led to increased flexibility, strength and barrier characteristics of the corn starch film, and the zein-rutin composite nanoparticle/corn starch film exhibited long-lasting antioxidant activity, which made them have potential application prospects in antioxidant activity packaging. Nanocellulose (NC) can be used as a reinforcing phase or as a matrix for a variety of materials including packaging films (Azeredo et al., 2017). Khan et al. (2012) found that as a good reinforcing agent, incorporation of NC significantly

improved the mechanical and barrier properties of the chitosan-based biodegradable films due to the strong filler-matrix interaction and the formation of a percolating network. Nano-TiO_2 (NT) is considered as a valuable nanometer material with nontoxicity, insipidity, thermostability, UV shielding ability and low price, which can be incorporated into the polymer matrix to modify the properties of biodegradable films (Goudarzi et al., 2017; Alizadeh-Sani, Khezerlou, & Ehsani, 2018). For example, sodium laurate-modified NT was successfully incorporated into chitosan/WPI film, and the glass transition temperature, enthalpy, whiteness, elongation at break and tensile strength of the film were increased by the nanoparticle (Zhang et al., 2016).

The addition of different nanoparticles may have different effects on the molecular network structure of KGM film, resulting in different performance changes. The aim of this paper is to evaluate the effect of nanoparticles (zein nanoparticles, nanocellulose, nano-TiO_2, nano-SiO_2) incorporation on the structural, thermal, mechanical and barrier properties of KGM based biodegradable films, and to investigate the effect of KGM/nanoparticles blend film on cherry tomatoes preservation. This information will provide promising suggestions for the production and application of KGM based nanocomposite films.

2. Materials and methods

2.1. Materials

Konjac glucomannan (KGM, M_w 1.012 × 10^6 g/mol; M_w/M_n 1.220; R(avg) 104.0 nm;

degree of acetylation 1.86%; molar ratio of glucose to mannose 1:1.6) was obtained from Konson Konjac Co., Ltd. (Hubei, China). Nano-SiO_2 (NS, analytical reagent, purity ≥ 99.5%; average particle size 10-20 nm), nano-TiO_2 (NT, analytical reagent, purity ≥ 99.8%, average particle size 5-10 nm) and α-cellulose (average particle size 25 μm) were purchased from Macklin Biochemical Co., Ltd. (Shanghai, China). Zein (M_w = 2.5-4.5 × 10^4 Da) was obtained from Beijing J & K Technology Co., Ltd. (Beijing, China). Span 80 (sorbitan monooleate) was purchased from Sinopharm Chemical Reagent Co., Ltd. (Shanghai, China). Cherry tomatoes of uniform texture and appearance were obtained from the local retail market. Other chemicals were analytical reagents.

2.2 Nanocellulose dispersion and zein nanoparticles preparation

Nanocellulose (NC) dispersion was prepared by the method described by Shankar and Rhim (2016) with slight modifications. α-cellulose (5.0 g) was dispersed in 100 mL of a solution containing 12% (w/v) urea and 7% (w/v) sodium hydroxide under stirring at 25 °C for 30 min. The obtained cellulose solution was kept at -20 °C for 16 h, then thawed, slowly dispersed in 200 mL of deionized water, and stirred at 1000 rpm for 10 min. Then it was sheared for 2 min at 19000 rpm by a homogenizer (Shanghai Fluke Technology Development Co., Ltd., China), suction-filtered, and washed with deionized water until the pH of the filtrate was 7. Deionized water of 400 mL was added to the filter residue and stirred at 1000 rpm for 10 min. Then, it was sheared at 19000 rpm for 2 min, and repeated 3 times to obtain NC dispersion. NC dispersion

was stored at 4 °C for subsequent experiments. The obtained NC was an irregular fibrous sheet structure with a length of 100-200 nm and a thickness of 10-20 nm.

Zein nanoparticles (NZ) were prepared based on the method described by Parris, Cooke and Hicks (2005) with minor modifications. Zein solution was obtained by dissolving 1.0 g of zein in 15 mL of 80% (v/v) ethanol/water solution. The zein solution was then added dropwise to 40 mL of deionized water while being sheared through a homogenizer at 19000 rpm. After the foam had formed on the top of the liquid, the foam was removed and the shear was continued for 2 min at 19000 rpm. After freeze-drying (Modulyod-230, Thermo Electron Corporation, USA), the NZ sample was obtained and stored in a desiccator. The obtained NZ was a spherical structure with a smooth surface and an average diameter of about 100 nm.

2.3 Films preparation

Five kinds of films were prepared, namely KGM film, KGM/nanocellulose blend film (KNC), KGM/zein nanoparticle blend film (KNZ), KGM/nano-SiO_2 blend film (KNS) and KGM/nano-TiO_2 blend film (KNT). Through preliminary experiments, the optimal formulation of the sample is shown in Table 1. The KGM film-forming solution was obtained by dissolving KGM in distilled water, adding glycerol, and stirring by electric mixer at 600 rpm for 0.5 h at 60 °C. The KNZ film-forming solution was obtained by dropping glycerol and NZ dispersion (adding NZ and Span 80 to 20 mL of 80% (v/v) ethanol/water solution) into KGM solution at 600 rpm for

0.5 h at 60 °C. The KNC film-forming solution was obtained by dispersing KGM and glycerol in NC dispersion with stirring speed at 600 rpm for 1.0 h at 60 °C. The KNT film-forming solution was prepared by adding glycerol and KGM to NT water dispersion at 800 rpm for 1.0 h at 60 °C. The KNS film-forming solution was obtained by adding glycerol and KGM to NS water dispersion at 600 rpm at 60 °C for 1.0 h. Then, the film-forming solution was evenly poured on the glass plate (15 cm × 16 cm × 1.5 cm) and dried at 60 °C in an oven until the moisture content was about 9% (w.b.). Before the test, all films were conditioned at 50 ± 2% relative humidity (RH) and 25 ± 1 °C for 48 h.

Table 1 The formulation of KGM film and KGM/nanoparticles blend films.

Samples / Elements	KGM	KNZ	KNC	KNT	KNS
KGM (g)	1.200	1.032	1.080	1.164	1.080
NZ (g)	-	0.168	-	-	-
NC (g)	-	-	0.120	-	-
NT (g)	-	-	-	0.036	-
NS (g)	-	-	-	-	0.120
Span 80 (g)	-	0.042	-	-	-
Glycerol (g)	0.240	0.240	0.240	0.240	0.240
Water (mL)	100	100	100	100	100
80% ethanol (mL)	-	20	-	-	-

2.4 Rheological analysis of film-forming solutions and characterization of films

The steady-state shear and dynamic rheological properties of film-forming solutions were evaluated according to the method of Ni et al. (2018). The microscopic morphology of films was observed with the Veeco multi-mode atomic force microscope (AFM, SPM9700, Shimadzu Co., Ltd., Japan) and a scanning electron

168 microscopy (SEM, Bio-Rad SC 502, JEOL, Tokyo, Japan) with reference to the
169 method described by Li, Wu, Su et al. (2019). The detection of Fourier transform
170 infrared spectroscopy (FTIR, Nicolet Avatar 360, Nicolet Co., USA) was based on the
171 method described by Wang et al. (2017). The glass transition temperature and the
172 thermal decomposition temperature were measured by a differential scanning
173 calorimeter (DSC, Mettler Toledo, Zurich, Switzerland) by the method described by
174 Wang et al. (2017).
175
176 The elongation at break (EAB, %) and tensile strength (TS, MPa) of films were
177 measured by a texture analyzer (TA. XT Plus, Stable Micro Systems Co., Ltd., UK)
178 according to the ASTM D882-09 standard method (ASTM, 2009). The film was cut
179 into a size of 1 cm × 3 cm, and the UV-visible absorption spectrum of the film was
180 recorded using a TU-1900 spectrophotometer (Beijing General Instrument Co., Ltd.,
181 China) from 280 to 580 nm. The water contact angle (WCA), solubility and swelling
182 in water, and water vapor permeability (WVP) of films were determined in
183 accordance with our previous methods (Li, Wu, Su et al., 2019). Oxygen barrier was
184 evaluated according to the following method (Wang et al., 2017; Meng et al., 2014).
185 Peanut oil (40 mL) was put into a polyethylene plastic cup, then sealed with the film
186 meticulously. The plastic cup was put in an incubator at 50 °C for 7 days, then the
187 peroxide value (P; mmol/kg) of peanut oil was measured according to Chinese
188 National Standard GB/T 5538-2005. The lower P reflects the better oxygen barrier of
189 the film.

2.5 Packaging and storage quality of cherry tomatoes

Taking cherry tomatoes as model fruits, the effect of KNZ film on their preservation was explored. There were three groups of samples: control group (CTC, without film packaging); cherry tomatoes wrapped in KNZ film (CTKNZ); cherry tomatoes wrapped in polyethylene (PE) film (CTPE). The samples were wrapped in films and heat sealed. The sensory and quality changes of cherry tomatoes during storage at 26 ± 1 °C, 37 ± 1% RH were analyzed.

Weight loss (%) was tested by deducting the sample's weight during specific storage (m_x) from its initial weight (m_0), and the formula was as follows: Weight loss = [(m_0 - m_x) / m_0] × 100%. Firmness (N/mm^2) was measured by a texture analyzer. The p/2 probe was used to penetrate the cherry tomato to a depth of 2 mm at a speed of 1.00 mm/sec.

Reverse osmosis water (65 g, cooled to 25 °C after boiling) was added to 35 g of cherry tomatoes (peel and pulp), and then crushed and filtered. The obtained filtrate was used for the determination of the content of total soluble solids (TSS), vitamin C (Vc) content and pH value. All operations were protected from light. TSS was observed by a digital Abbe refractometer (Model WAY-2S, Shanghai Jingke Industrial Co., Ltd., China). The sample was placed directly on the refractometer for testing (> 2 drops). The method of Vc measurement referred to Nejati-Yazdinejad (2007). The pH of the sample was tested by a digital pH meter (DELTA 320, Mettler Tori Instrument

213 Co., Ltd., Shanghai, China).

214

215 ***2.6 Statistical analysis***

216 Each experiment was carried out at least three times. Graph drawing and statistical
217 analysis were performed by Origin 2017 (OriginLab Corporation, USA). One-way
218 analysis of variance was conducted using the SPSS software (19^{th} edition, Endicott,
219 NY, USA) by Tukey's multiple range test with $p < 0.05$.

220

221 **3. Results and discussion**

222 ***3.1. Rheological properties of film-forming solutions***

223 The rheological characteristics of film-forming solutions are important for controlling
224 the preparation of films and understanding the structure and physicochemical
225 properties of films. In Fig. 1 A, the apparent viscosity (η) of KGM solution (1.2%)
226 and other blended film-forming solutions decreased with the increase of shear rate,
227 showing shear-thinning behavior. The entanglement effect plays a key role in the
228 rheological behavior of linear polymers (Tanaka et al., 2005). In the entangled
229 network system formed by KGM linear molecules, the shear-thinning behavior can be
230 attributed to the fact that the rate of re-entanglement is lower than the rate of
231 destruction of existing entanglement caused by shear, resulting in a decrease in
232 viscosity with increasing shear strength (Graessley, 1974). The η values of blend
233 film-forming solutions decreased gradually with the decrease of the KGM
234 concentration. The non-Newtonian, shear-thinning behavior of film-forming solutions

was mainly attributed to the KGM component.

Changes in storage modulus (G′) and loss modulus (G") with angular frequency (ω) for film-forming solutions are shown in Fig. 1 (B-F). The G′ and G" of all samples increased with the increase of ω and had a crossover, showing frequency-dependent. It was considered as a typical behavior of entangled polymer solution (Nishinari, 2009, 1997). G" was larger than G′ at lower frequencies, suggesting liquid-like properties; whereas G′ predominated G" at higher frequencies, indicating that the solution transformed to an elastic solid. This could be explained by that the molecular chains could disentangle in the process of long-term oscillation at low frequencies, and the solution behaved as viscous liquid; while at high frequencies, the molecular chains could not disentangle during short-time oscillation, and as a result, the behavior of the solution tended to be an elastic solid (Nishinari, 1997). Their entanglement points acted as temporary knots in the three-dimensional network. Compared with KGM solution, the crossover point of blend solutions shifted to high frequencies, indicating weakened hydrogen bonding and entanglement. This might be due to the lower KGM content leading to less hydrogen bonding, which reduced the chance of macromolecular chain entanglement. In blend solutions, the crossover point of KNZ film-forming solution showed the lowest frequency value, although its KGM content was the lowest. This indicated that the strongest interaction between NZ and KGM molecules might have occurred, enhancing the entanglement of molecular chains.

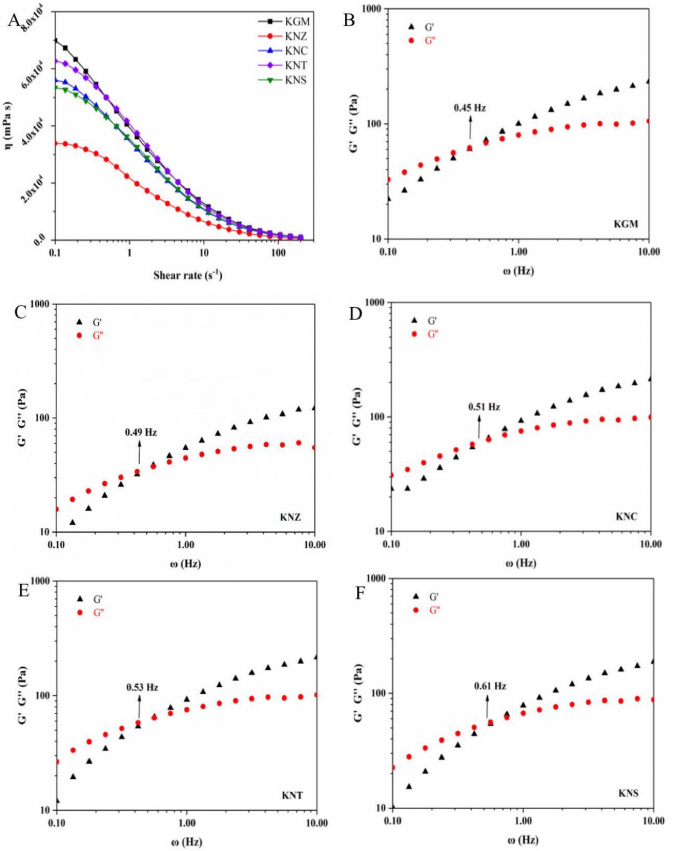

Fig. 1. Steady (A) and dynamic (B, C, D, E, F) rheological curves of the KGM film-forming solution and blend film-forming solutions.

3.2. Microstructure of films

Fig. 2 shows the typical AFM topography images of KGM film and

KGM/nanoparticles blend films. KGM film had a smoother and more homogeneous surface compared with the blend films. The addition of nanoparticles increased the average roughness (Ra) of the films from 8.65 to 37.82 nm. Among the blend films, KNS had the highest Ra (37.82 nm), which might be due to the aggregation of NS into larger particles. KNZ had the lowest Ra (11.65 nm), indicating that KNZ had a more uniform and denser surface than other blend films, and there might be a good interaction between KGM and NZ, which would contribute to the better mechanical and physical properties of KNZ.

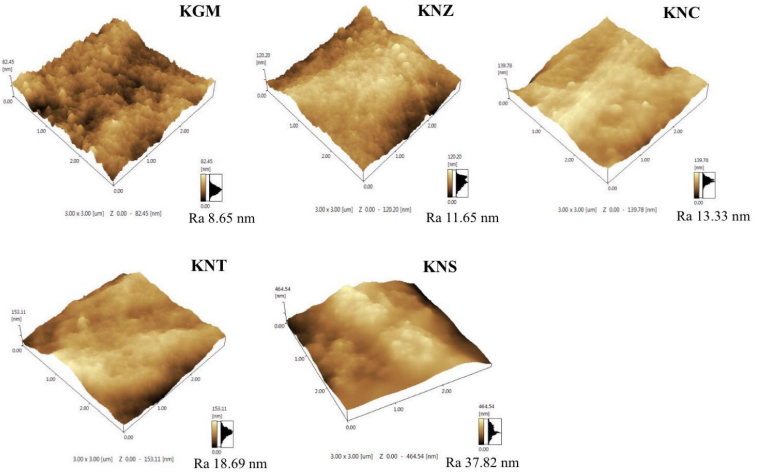

Fig. 2. The three-dimensional images of AFM of KGM, KNZ, KNC, KNT and KNS films.

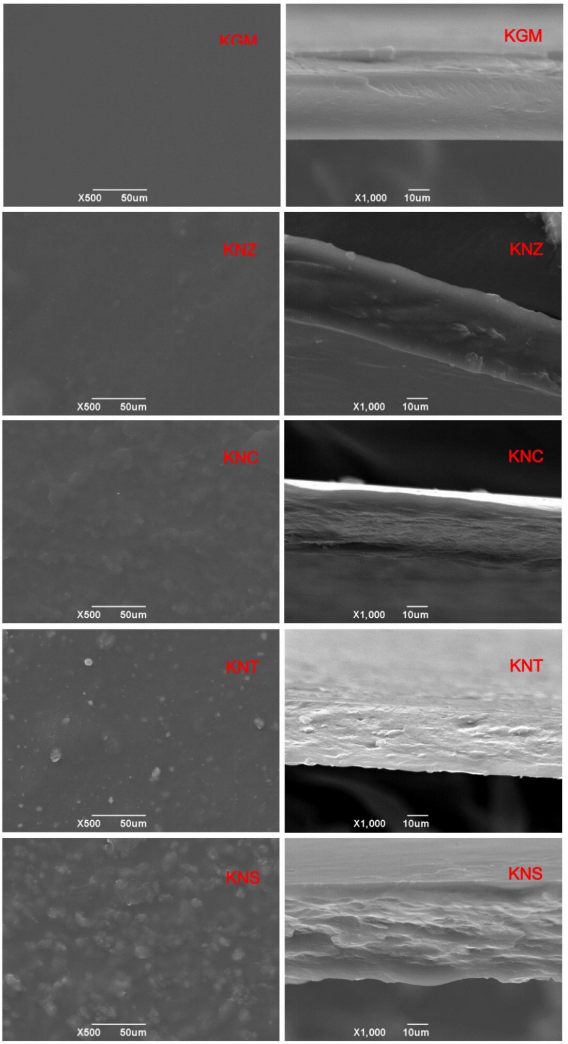

Fig. 3. The scanning electron microscope photos of the surface and cross-section of KGM, KNZ, KNC, KNT and KNS films.

The microstructure of films was further examined by SEM (Fig. 3). Among all samples, the surface and cross-section of pure KGM film exhibited the smoothest and densest structure. In blend films, NZ, NC, NT and NS were evenly distributed in the KGM matrix respectively, destroying the original structure of KGM film. The surface and cross-section of KNZ were relatively smooth and compact, due to the distribution of small NZ aggregates, which was consistent with the AFM results. For KNC, the small pieces aggregated by NC were embedded in its surface, and its cross-section presented a loose layered structure. The surface of KNS and KNT was rougher than that of KNZ and KNC, and the cross-section of KNS showed discontinuous and loose structure with large particles. It was speculated from the SEM images that the incorporation of nanoparticles to KGM film might lead to more complex network channels and better barrier effect on external small molecules (such as O_2, H_2O, etc.) (Lin et al., 2020; Peighambardoust et al., 2019).

3.3. FTIR analysis, thermal and UV absorption properties of films

The FTIR spectra of KGM, KNZ, KNC, KNT and KNS films in the rage of 4000-650 cm^{-1} are shown in Fig. 4 A. In KGM film, the broad absorption bands at 3320 cm^{-1} and 2918 cm^{-1} were attributed to -OH stretching vibration and C-H stretching vibration. The absorption band at 1645 cm^{-1} corresponded to intramolecular hydrogen bonds. The absorption bands at 875 cm^{-1} and 806 cm^{-1} were the characteristic absorption peaks of mannose unit. These absorption bands were consistent with the reports by Li et al. (2015) and Wu et al. (2012). For KGM/nanoparticles blend films,

300 the broad bands of -OH stretching vibration (3400-3200 cm^{-1}) shifted gradually to
301 lower wavenumbers compared with that of KGM film, indicating occurrence of
302 hydrogen bond interactions between KGM and the nanoparticles in the blend films,
303 similar to KGM/curdlan blend films (Wu et al., 2012).
304
305 The thermal properties of the films changed significantly with the addition of
306 nanoparticles according to the DSC curves (Fig. 4 B). In Fig. 4 B, KGM film
307 presented obvious endothermic peak at 79.8 °C, which corresponded to its glass
308 transition temperature (T_g), consistent with reported results (Wang et al., 2017). KNZ,
309 KNC, KNT and KNS showed T_g at 120.9, 111.7, 110.3 and 109.2 °C, respectively.
310 The higher the T_g, the higher the temperature required to break the molecular chain,
311 suggesting enhanced molecular interaction (Ahmad et al., 2015). The intermolecular
312 interactions between KGM and the nanoparticles may change the original crystalline
313 structure and molecular network, resulting in higher T_g values than that of KGM film.
314 Zuo et al. (2020) reported that nano-SiO_2 addition improved the crystallinity of the
315 polylactic acid-grafted-bamboofiber/polylactic acid composites, and the increase in
316 crystallinity made the composites have better heat resistance. Moreover, the blend
317 films all exhibited a single T_g, which indicated good miscibility/compatibility between
318 the film components (Biliaderis, Lazaridou, & Arvanitoyannis, 1999; Li et al., 2015).
319 According to the DSC curves, the thermal decomposition temperature (T_d) of KGM,
320 KNZ, KNC, KNT and KNS films were 318.9, 334.5, 323.1, 322.8, and 319.0 °C,
321 respectively. Changes in T_g and T_d indicated that the addition of nanoparticles

improved the heat resistance of the blend films, and KNZ showed the strongest thermal stability due to the strongest molecular interaction.

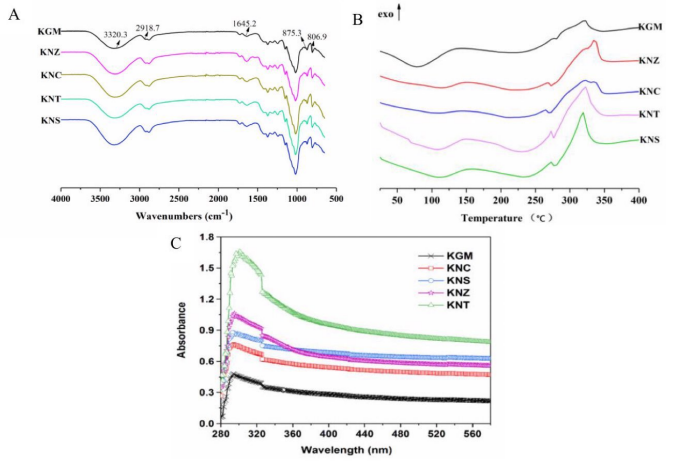

Fig. 4. The FTIR curves (A), DSC curves (B) and UV-visible absorption spectra curves (C) of KGM, KNZ, KNC, KNT and KNS films.

The UV-visible absorption spectrum can be used to evaluate the transparency of the film against visible light and the shielding effect of the film on ultraviolet rays (Fig. 4 C). As shown, when the nanoparticles were added to the KGM matrix, the transmittance of blend films was significantly lower than that of pure KGM film, indicating that these nanoparticles had good shielding effect in both visible and UV ranges. The reduced transparency of the blend films might be due to the interactions between the nanoparticles and the KGM matrix, which caused the accumulation of polymer chains and the increase of crystallinity, leading to changes in refractive index

and interference with light transmission. In addition, the presence of nanoparticles in the matrix may result in increased light scattering through the film (Farajpour et al., 2020). The UV shielding effect of the film mainly depended on the UV-absorbing material with a wavelength of 280-315 nm. Compared with pure KGM film, the UV shielding effect of blend films was improved, and KNT showed the best UV shielding effect. This can be explained as NT is a direct wide-band-gap semiconductor with a special function of ultraviolet absorption (Goudarzi, Shahabi-Ghahfarrokhi, & Babaei-Ghazvin, 2017).

3.4. Mechanical properties of films

Adding the nanoparticles to the KGM matrix had no obvious effect on the film thickness (Table 2), and the thickness of KNT and KNS slightly increased. This might be due to looser film structure caused by NT and NS, which was consistent with the results of SEM. The TS and EAB of the blend films increased significantly compared to pure KGM film, indicating the enhancement of the mechanical properties, as shown in Table 2. This can be attributed to the well-dispersed nanoparticles, the interactions and good compatibility between KGM and the nanoparticles, in agreement with previous discussions. The TS value of KNT was the largest, reaching 82.6 MPa, which increased by 97.14% compared with that of KGM film. Some researchers reported that the addition of NT resulted in the mechanical strengthening of chitosan matrices, especially the improvement of Young's modulus and TS, without affecting considerably the EAB (Amin, & Panhuis, 2012; Mallakpour, & Madani, 2015). While

the largest EAB value appeared in KNZ (increased by 148.0%). The nanoparticles were filled in the polymer matrix like a ball bearing, which increased the mobility of the polymer chains and made the movement of the nanocomposite chains easier than that for virgin polymer chains (Shahabi-Ghahfarrokhi et al., 2015; Goudarzi, et al., 2017). Furthermore, studies had reported that the plasticization of NZ led to the increase of spacing and mobility between chains by mitigating the effect of polymer chains interactions (Oymaci, & Altinkaya, 2016).

371

372 **Table 2** The mechanical properties, water contact angle, swelling, solubility, WVP and oxygen barrier of the films.

Indexes / Samples	Thickness (μm)	Tensile strength (MPa)	Elongation at break (%)	Water contact angle (°)	Swelling (%)	Solubility (%)	WVP (10^{-13}·g·cm/(cm^2·s·Pa))	P (mmol/kg)
KGM	38.0 ± 1.8^{a}	41.9 ± 3.2^{a}	20.0 ± 3.1^{a}	37.3 ± 2.5^{a}	-	-	11.8 ± 0.5^{d}	2.8 ± 0.1^{a}
KNZ	39.0 ± 1.2^{a}	68.8 ± 5.9^{b}	49.6 ± 6.3^{c}	94.1 ± 1.0^{b}	1218.9 ± 49.5^{a}	22.7 ± 2.6^{a}	9.5 ± 0.3^{ab}	2.4 ± 0.1^{bc}
KNC	39.0 ± 1.8^{a}	63.5 ± 3.3^{b}	39.8 ± 3.6^{b}	97.4 ± 1.4^{b}	1462.5 ± 71.5^{a}	28.7 ± 3.0^{a}	9.2 ± 0.3^{a}	2.2 ± 0.2^{c}
KNT	41.8 ± 1.7^{ab}	82.6 ± 5.7^{c}	37.7 ± 2.4^{b}	50.5 ± 2.6^{c}	3373.6 ± 200.8^{b}	39.9 ± 1.6^{b}	10.1 ± 0.3^{bc}	2.3 ± 0.1^{c}
KNS	43.8 ± 1.7^{ab}	60.6 ± 5.3^{b}	25.3 ± 3.2^{ab}	49.2 ± 1.1^{c}	3405.2 ± 200.9^{b}	41.4 ± 0.6^{b}	10.8 ± 0.3^{c}	2.6 ± 0.1^{b}

373 Different superscripts (a-d) in the column indicate significant differences ($p < 0.05$). The value is the mean ± standard deviation.

374

3.5. Surface hydrophobicity, swelling and solubility properties of films

Water contact angle (WCA) is an important index to characterize the wettability of the film surface. The greater the water contact angle value, the stronger the surface hydrophobicity of the film (Shankar, & Rhim, 2016; Yin et al., 2014). The WCA values of KGM, KNZ, KNC, KNT, and KNS films are shown in Table 2. KGM is a kind of polysaccharide with strong hydrophilicity, which is easy to absorb water in an aqueous environment. Therefore, pure KGM film had the smallest WCA, reflecting its low hydrophobicity. With the addition of nanoparticles (NZ, NC, NT and NS), the WCA values of the blend films increased significantly, while the WCA values of KNZ and KNC were the largest. The increase in the hydrophobicity of the blend films was mainly due to the enhanced intermolecular interaction and the increase in hydrophobic components in the film (Oymaci, & Altinkaya, 2016). Similar to our study, some studies had shown that the WCA of nanocomposite films was increased, e.g. nanocomposite starch (Goudarzi, Shahabi-Ghahfarrokhi, & Babaei-Ghazvini, 2017), nanocomposite chitosan (Khan et al., 2012) and nanocomposite whey protein isolate (Oymaci, & Altinkaya, 2016). Due to the high surface energy and large specific surface area of nanoparticles, more energy was required for the diffusion of water droplets on them, which was reflected in the increase of WCA (Zuo et al., 2020). The hydrophobicity of NZ and NC was stronger than that of NT and NS, resulting in better surface hydrophobicity of KNZ and KNC. In addition, the aggregation of NT and NS may reduce their original large surface area and nano effects.

The swelling and solubility properties reflect the stability of the film in an aqueous environment, demonstrating the hydrophobicity from practical aspects. Due to the rapid dissolution and dispersion in water, pure KGM film was not suitable for testing. The addition of nanoparticles significantly enhanced the water resistance of the blend films (Table 2). KNZ and KNC exhibited the greatest hydrophobicity due to the lowest swelling ratio and solubility, similar to the WCA results. This phenomenon can be ascribed firstly to the low water uptake of the NZ and NC themselves; and secondly to the creation of strong network structures (Alizadeh-Sani, Khezerlou, & Ehsani, 2018). Meanwhile, due to the aggregation of NT and NS, the surface roughness of KNT and KNS was greater than that of KNZ and KNC, and the effective hydrophobic surface area of KNT and KNS was reduced (Bayat, Ebrahimi, & Moshfegh, 2014; Gilbert, Cheng, & Jones, 2018). Therefore, more KGM molecules may be exposed to water environment, reducing the hydrophobicity of KNT and KNS.

3.6. Water vapor permeability (WVP) and oxygen barrier of films

In order to apply the film to packaging, it must have good barrier performance. The lower the WVP and peroxide value (P), the less the possibility of water and oxygen molecules penetrating the film, and the better the barrier of water and oxygen. It could be seen from Table 2 that the WVP and P of KNZ, KNC, KNT and KNS were significantly lower than those of pure KGM film, suggesting that the barrier properties of blend films were better than those of pure KGM film. For WVP, this may be due to

the fact that the nanoparticles in the blend films act as an impermeable barrier for the penetration of water vapor, increasing the tortuous path for water vapor to diffuse through the films, resulting in a decrease in the WVP of the blend films (Shankar, & Rhim, 2016; Alizadeh-Sani, Khezerlou, & Ehsani, 2018). In addition, the hydrophilicity of the film and the presence of pores in the film also affected the WVP. KNZ and KNC showed the smallest WVP, which was due to the strong hydrophobic nature of both NZ and NC and the dense film structure of KNZ and KNC. Oxygen barrier of films depends largely on the interaction between oxygen and polymer matrix, as well as the film microstructure (García, Martino, & Zaritzky, 2000). The change in P (Table 2) may reflect the difference in the microstructure of films. The KNS showed higher P among the blend films, indicating that more oxygen penetrated the film to oxidize the oil, which might be attributed to the loose structure with presence of pores and cracks in the KNS observed by SEM.

Fig. 5. The visual quality with storage from the 6th to 10th day of cherry tomatoes (stored at 26 ± 1 °C, 37 ± 1% RH).

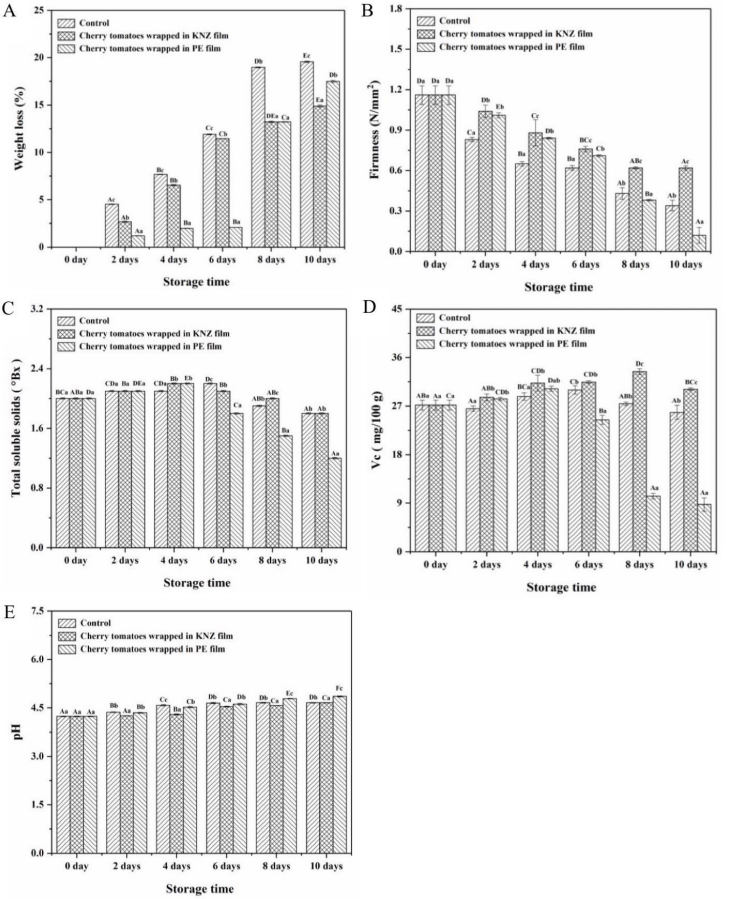

Fig. 6. The weight loss (A), firmness (B), TSS (C), Vc (D) and pH (E) of cherry tomatoes during the storage (stored at 26 ± 1 °C, 37 ± 1% RH).

Different letters (a-c) represent the significant difference of different samples in the same storage time, and different letters (A-F) represent the significant difference of the same sample in different storage time ($p < 0.05$).

3.7 Effect of KNZ film on cherry tomatoes preservation

Through a comprehensive comparison of the physicochemical properties of KNZ, KNC, KNT and KNS films, KNZ film showed the best performance and was selected for cherry tomatoes packaging. Cherry tomatoes are climacteric fruits, and their postharvest life is relatively short, so proper packaging is beneficial to extend their shelf life. Appearance change is the most intuitive way to evaluate the quality of cherry tomatoes. When the storage time reached 6 days, there were significant differences in appearance of cherry tomatoes with different packaging in Fig. 5. For CTC group, on the 6^{th} day of storage, cherry tomatoes lost moisture obviously and their surface was wrinkled due to exposure to air. As the storage days prolonged, the moisture loss of the sample became more serious. On the 10^{th} day, the surface of the sample showed severe shrinkage and decay, but no obvious mildew was seen. Mold mycelium began to appear on the surface of CTPE on the 6^{th} day, and there was obvious condensation on the inner wall of PE film. CTPE suffered severe moisture loss and decay on the 8^{th} day. CTKNZ remained fresh during 10 days of storage. A good atmosphere in the package can slow down product respiration rate and delay product deterioration, which is affected by the interplay of product respiration, package permeability and storage temperature. Therefore, matching the film permeability to the product characteristics and creating an atmosphere suitable for the product is very important to extend the shelf life (Paulsen, Barrios, & Lema, 2019). Cherry tomatoes were in an independent environment after being wrapped in the film.

It might be that PE film prevented moisture exchange with the outside, which increased the humidity inside the package and formed an environment conducive to the growth of mold. KNZ film created an improved atmosphere due to good vapor permeability, thus providing a good storage environment for cherry tomatoes.

Fig. 6 A showed that the weight loss of CTC was significantly higher than that of CTPE and CTKNZ during the storage, reaching 19.56% on the 10^{th} day. It might be because CTC was directly exposed to air, which accelerated their moisture migration. CTPE and CTKNZ were well packed, which slowed down the respiration and transpiration of cherry tomatoes, resulting in lower weight loss. On the 8^{th} day, CTPE ruptured due to deterioration and the cherry tomato juice flowed out, and weight loss increased rapidly. After the 8^{th} day, the weight loss of CTPE was greater than that of CTKNZ. The firmness of fruit is an important factor affecting consumer acceptance and product shelf life. The firmness of all samples showed a decreasing trend, and CTKNZ had the best firmness during the storage based on Fig. 6 B. On the 8^{th} day of storage, CTPE became significantly softer than CTC and CTKNZ. This may be due to moisture loss and decay, resulting in a softer texture of cherry tomatoes.

TSS increased with the maturity and senescence of fruits due to the hydrolysis of insoluble polysaccharides into monosaccharides (Sammi, & Masud, 2009). The smaller the change of TSS, the better the preservation effect (Aragüez et al., 2020). From Fig. 6 C, it was found that TSS of CTC increased (before the 6^{th} day), and then

512 began to decrease (the 8th day), the tendency was similar to the reports by
513 Tumwesigye et al. (2017). For CTPE, TSS decreased significantly from 2.2 °Bx (the
514 4th day) to 1.8 °Bx (the 6th day), 1.5 °Bx (the 8th day) and 1.2 °Bx (the 10th day). The
515 reason might be that the growing mold absorbed nutrients, resulting in a significant
516 decrease in TSS of cherry tomatoes (Li, Xu, Bi et al., 2019). However, for CTKNZ,
517 TSS did not change significantly during 10 days of storage. It may be that KNZ
518 packaging can regulate or suppress the respiration and transpiration of cherry
519 tomatoes, resulting in no significant changes in TSS of cherry tomatoes.
520
521 It could be seen from Fig. 6 D that during the storage, the Vc content increased first
522 and then decreased. This phenomenon was similar to the results of Wu et al. (2016).
523 Before the 4th day of storage, the Vc content was in the rising stage. It was speculated
524 that cherry tomatoes went through the post-ripening (Zhou et al., 2019). Before the 4th
525 day, the content of Vc in CTC was lower than that of other groups, which might be
526 due to direct exposure to air, resulting in a rapid decline in the postharvest quality
527 (Guo et al., 2020). After the 6th day, the Vc content of CTPE decreased significantly.
528 This was because CTPE began to rupture due to deterioration, causing Vc to be easily
529 exposed to oxygen and oxidized; meanwhile, the outflow of cherry tomato juice also
530 led to the loss of Vc. During the whole storage, the Vc content of CTKNZ was higher
531 than that of other groups. This might be due to the good barrier effect of KNZ on
532 oxygen and ultraviolet, which could alleviate the oxidative damage and keep the Vc
533 content of cherry tomatoes at a high value. Fig. 6 E showed that the pH of the samples

all increased during the storage. It might be that cherry tomatoes used organic acids as respiratory substrates, resulting in a decrease in acidity and an increase in pH (Tumwesigye et al., 2017). The pH values of CTC and CTKNZ were stable after the 6^{th} day, but the pH of CTPE increased. On the 10^{th} day, the pH of CTC and CTKNZ was maintained between 4.5-4.6, and the pH of CTPE increased to 4.8. The increase in the pH of CTPE may be related to the growth of mold.

The above analysis suggested that KNZ film packaging could cut down the weight loss and firmness reduction of cherry tomatoes during the storage, and sustain the TSS, Vc content and pH value.

4. Conclusions

With appropriate formulations, KGM/nanoparticles blend films were prepared by solution casting. The blend film-forming solutions exhibited shear-thinning behavior and were typical entangled polymer solutions. KGM/zein nanoparticle film-forming solution showed the lowest crossover of G′ and G", indicating enhanced molecular interaction and entanglement. The nanoparticles (NZ, NC, NT, NS) were dispersed homogeneously in the KGM matrix, and interactions occurred between the nanoparticles and KGM molecules, and there was good compatibility. The addition of nanoparticles improved the thermal stability, mechanical, hydrophobic, water vapor and oxygen barrier, UV shielding properties of KGM based films. However, different nanoparticles had different effects on the performance of KGM based films. The KNZ

showed the best properties, such as the highest glass transition temperature and elongation at break, as well as the best moisture and oxygen barrier, due to its densest structure and strongest molecular interaction. Cherry tomatoes in KNZ film packaging showed lower quality changes and longer shelf life compared with those in PE film packaging during the storage at 26 °C.

CRediT authorship contribution statement

Fei Xiang: Investigation, Methodology, Writing - original draft. **Yuting Xia**: Investigation, Validation. **Yan Wang**: Investigation, Validation. **Yixin Wang**: Investigation, Review. **Kao Wu**: Data curation, Software. **Xuewen Ni**: Project administration, Methodology, Conceptualization, Funding acquisition, Writing - review & editing.

Acknowledgements

This work was sponsored by Green Technology Program of Hubei University of Technology, Approval Number CPYF2018004.

References

Ahmad, M., Hani, N. M., Nirmal, N. P., Fazial, F. F., Mohtar, N. F., & Romli, S. R. (2015). Optical and thermo-mechanical properties of composite films based on fish gelatin/rice flour fabricated by casting technique. *Progress in Organic Coatings, 84*, 115-127.

Alizadeh-Sani, M., Khezerlou, A., & Ehsani, A. (2018). Fabrication and characterization of the bionanocomposite film based on whey protein biopolymer loaded with TiO_2 nanoparticles, cellulose nanofibers and

rosemary essential oil. *Industrial Crops and Products, 124*, 300-315.

Amin, K. A. M., & Panhuis, M. (2012). Reinforced materials based on chitosan, TiO_2 and Ag composites. *Polymers, 4*(1), 590-599.

Aragüez, L., Colombo, A., Borneo, R., & Aguirre, A. (2020). Active packaging from triticale flour films for prolonging storage life of cherry tomato. *Food Packaging and Shelf Life*, *25*, 100520.

ASTM. (2009). Standard test method for tensile properties of thin plastic sheeting, vol. ASTM D882-09 (West Conshohocken, PA).

Azeredo, H. M. C., Rosa, M. F., & Mattoso, L. H. C. (2017). Nanocellulose in bio-based food packaging applications. *Industrial Crops and Products, 97*, 664-671.

Bayat, A., Ebrahimi, M., & Moshfegh, A. Z. (2014). Correlation between surface roughness and hydrophobicity of GLAD RF Sputtered PTFE/W/Glass nanorod thin films. *Vacuum, 101*, 279-282.

Biliaderis, C. G., Lazaridou, A., & Arvanitoyannis, I. (1999). Glass transition and physical properties of polyol-plasticised pullulan–starch blends at low moisture. *Carbohydrate Polymers, 40*(1), 29-47.

Castro-Rosas, J., Cruz-Galvez, A. M., Gomez-Aldapa, C. A., Falfan-Cortes, R. N., Guzman-Ortiz, F. A., & Rodríguez-Marín, M. L. (2016). Biopolymer films and the effects of added lipids, nanoparticles and antimicrobials on their mechanical and barrier properties: a review. *International Journal of Food Science and Technology, 51*(9), 1967-1978.

Chen, J., Liu, C., Chen, Y., Chen, Y., & Chang, P. (2008). Structural characterization and properties of starch/konjac glucomannan blend films. *Carbohydrate Polymers, 74*(4), 946-952.

Farajpour, R., Djomeh, Z. E., Moeini, S., Tavakolipour, H., & Safayan, S. (2020). Structural and physico-mechanical properties of potato starch-olive oil edible films reinforced with zein nanoparticles. *International Journal of Biological Macromolecules, 149*(15), 941-950.

García, M. A., Martino, M. N., & Zaritzky, N. E. (2000). Lipid addition to improve barrier properties of edible starch-based films and coatings. *Journal of Food Science, 65*(6), 941-944.

GB/T 5538-2005. (2005). Method for determination of peroxide value of animal and vegetable oils.

Gilbert, J., Cheng, C. J., & Jones, O. G. (2018). Vapor barrier properties and mechanical behaviors of composite hydroxypropyl methylcellulose/zein nanoparticle films. *Food Biophysics, 13*(1), 25-36.

Goudarzi, V., Shahabi-Ghahfarrokhi, I., & Babaei-Ghazvini, A. (2017). Preparation of ecofriendly UV-protective food packaging material by starch/TiO_2 bio-nanocomposite: Characterization. *International Journal of Biological Macromolecules, 95*, 306-313.

Graessley, W. W. (1974). The entanglement concept in polymer rheology. *Advances in Polymer Science, 16*, 1-179.

Guo, X., Chen, B., Wu, X., Li, J., & Sun, Q. (2020). Utilization of cinnamaldehyde and zinc oxide nanoparticles in a carboxymethylcellulose-based composite coating to improve the postharvest quality of cherry tomatoes. *International Journal of Biological Macromolecules, 160*(1), 175-182.

Kato, K., & Matsuda, K. (1969). Studies on the chemical structure of konjac mannan: Part I. Isolation and characterization of oligosaccharides from the partial acid hydrolysate of the mannan. *Agricultural and biological chemistry, 33*, 1446-1453.

Khan, A., Khan, R. A., Salmieri, S., Tien, C. L., Riedl, B., Bouchard, J., et al. (2012). Mechanical and barrier properties of nanocrystalline cellulose reinforced chitosan based nanocomposite films. *Carbohydrate Polymers, 90*(4), 1601-1608.

Leuangsukrerk, M., Phupoksakul, T., Tananuwong, K., Borompichaichartkul, C., & Janjarasskul, T. (2014). Properties of konjac glucomannan-whey protein isolate blend films. *LWT - Food Science and Technology, 59*(1), 94-100.

Li, C., Wu, K., Su, Y., Riffat, S. B., Ni, X., & Jiang, F. (2019). Effect of drying temperature on structural and thermomechanical properties of konjac glucomannan-zein blend films. *International Journal of Biological Macromolecules, 138*(1), 135-143.

Li, H., Wang, D., Liu, C., Zhu, J., Fan, M., Sun, X., et al. (2019). Fabrication of stable zein nanoparticles coated with soluble soybean polysaccharide for encapsulation of quercetin. *Food Hydrocolloids, 87*, 342-351.

668 Li, S., Xu, Y., Bi, Y., Zhang, B., Shen, S., Jiang, T., et al. (2019). Melatonin treatment
669 inhibits gray mold and induces disease resistance in cherry tomato fruit
670 during postharvest. *Postharvest Biology and Technology, 157*, 110962.
671
672 Li, X., Jiang, F., Ni, X., Yan, W., Fang, Y., Corke, H., et al. (2015). Preparation and
673 characterization of konjac glucomannan and ethyl cellulose blend films.
674 *Food Hydrocolloids. 44*, 229-236.
675
676 Lin, Q., Ji, N., Li, M., Dai, L., Xu, X., Xiong, L., & Sun, Q. (2020). Fabrication of
677 debranched starch nanoparticles via reverse emulsification for improvement
678 of functional properties of corn starch films. *Food Hydrocolloids, 104*,
679 105760.
680
681 Mallakpour, S., & Madani, M. (2015). Effect of functionalized TiO_2 on mechanical,
682 thermal and swelling properties of chitosan-based nanocomposite films.
683 *Polymer-Plastics Technology and Engineering, 54*(10), 1035-1042.
684
685 Meng, T., Liu, D., Li, H., Ou, J., Hao, Z., & Zhang, H. (2014). Processing technology
686 of edible composite membranes. *Soybean Science*, *33*(2), 277-280.
687
688 Nejati-Yazdinejad, M. (2007). Indirect determination of ascorbic acid (vitamin C) by
689 spectrophotometric method. *International Journal of Food Science &*
690 *Technology, 42*(12), 1402-1407.
691
692 Nishinari, K. (2009). Some thoughts on the definition of a gel. *Progress in Colloid &*
693 *Polymer Science, 136*, 87-94.
694
695 Nishinari, K. (1997). Rheological and DSC study of sol-gel transition in aqueous
696 dispersions of industrially important polymers and colloids. *Colloid and*
697 *Polymer Science, 275*(12), 1093-1107.
698
699 Ni, X., Wang, K., Wu, K., Corke, H., Nishinari, K., & Jiang, F. (2018). Stability,
700 microstructure and rheological behavior of konjac glucomannan-zein mixed
701 systems. *Carbohydrate Polymers, 188*(15), 260-267.
702
703 Oymaci, P., & Altinkaya, S. A. (2016). Improvement of barrier and mechanical
704 properties of whey protein isolate based food packaging films by
705 incorporation of zein nanoparticles as a novel bionanocomposite. *Food*
706 *Hydrocolloids, 54*, 1-9.
707
708 Parris, N., Cooke, P. H., & Hicks, K. B. (2005). Encapsulation of essential oils in zein
709 nanospherical particles. *Journal of Agricultural and Food Chemistry, 53*(12),
710 4788-4792.

Paulsen, E., Barrios, S., & Lema, P. (2019). Ready-to-eat cherry tomatoes: Passive modified atmosphere packaging conditions for shelf life extension. *Food Packaging and Shelf Life, 22,* 100407.

Peighambardoust, S. J., Peighambardoust, S. H., Pournasir, N., & Pakdel, P. M. (2019). Properties of active starch-based films incorporating a combination of Ag, ZnO and CuO nanoparticles for potential use in food packaging applications. *Food Packaging and Shelf Life, 22*, 100420.

Rhim, J. W., & Ng, P. K. W. (2007). Natural biopolymer-based nanocomposite films for packaging application. *Critical Reviews in Food Science and Nutrition, 47*(4), 411-433.

Sammi, A., & Masud, T. (2009). Effect of different packaging systems on the quality of tomato (Lycopersicon esculentumvar. Rio Grande) fruits during storage. *International Journal of Food Science and Technology, 44*(5), 918-926.

Shahabi-Ghahfarrokhi, I., Khodaiyan, F., Mousavi, M., & Yousefi, H. (2015). Preparation of UV-protective kefiran/nano-ZnO nanocomposites: physical and mechanical properties. *International Journal of Biological Macromolecules, 72*, 41-46.

Shankar, S., & Rhim, J. W. (2016). Preparation of nanocellulose from micro-crystalline cellulose: The effect on the performance and properties of agar-based composite films. *Carbohydrate Polymers, 135*(1), 18-26.

Tanaka, H., Nishikawa, Y., & Koyama, T. (2005). Network-forming phase separation of colloidal suspensions. *Journal of Physics: Condensed Matter, 17*(15), 143-153.

Tang, H., Xiong, H., Tang, S., & Zou, P. (2009). A starch-based biodegradable film modified by nano silicon dioxide. *Journal of Applied Polymer Science, 113*(1), 34-40.

Tumwesigye, K. S., Sousa, A. R., Oliveira, J. C., & Sousa-Gallagher, M. J. (2017). Evaluation of novel bitter cassava film for equilibrium modified atmosphere packaging of cherry tomatoes. *Food Packaging and Shelf Life, 13,* 1-14.

Wang, K., Wu, K., Xiao, M., Kuang, Y., Corke, H., Ni, X., et al. (2017). Structural characterization and properties of konjac glucomannan and zein blend films. *International journal of biological macromolecules, 105*(1), 1096-1104.

Wu, C., Peng, S., Wen, C., Wang, X., Fan, L., Deng, R., et al. (2012). Structural characterization and properties of konjac glucomannan/curdlan blend films. *Carbohydrate Polymers, 89*(2), 497-503.

Wu, S., Lu, M., & Wang, S. (2016). Effect of oligosaccharides derived from Laminaria japonica-incorporated pullulan coatings on preservation of cherry tomatoes. *Food Chemistry, 199*(15), 296-300.

Xiao, C., Lu, Y., Gao, S., & Zhang, L. (2001). Characterization of konjac glucomannan-gelatin blend films. *Journal of Applied Polymer Science, 79*(9), 1596-1602.

Yoshimura, M., & Nishinari, K. (1999). Dynamic viscoelastic study on the gelation of konjac glucomannan with different molecular weights. *Food Hydrocolloids, 13*(3), 227-233.

Yin, Y., Yin, S., Yang, X., Tang, C., Wen, S., Chen, Z., et al. (2014). Surface modification of sodium caseinate films by zein coatings. *Food Hydrocolloids, 36*(2), 1-8.

Zhang, S., & Zhao, H. (2017). Preparation and properties of zein-rutin composite nanoparticle/corn starch films. *Carbohydrate Polymers*, *169*(1), 385-392.

Zhang, W., Chen, J., Chen, Y., Xia, W., L. Xiong, Y., & Wang, H. (2016). Enhanced physicochemical properties of chitosan/whey protein isolate composite film by sodium laurate-modified TiO_2 nanoparticles. *Carbohydrate Polymers, 138*(15), 59-65.

Zhou, X., Yang, R., Wang, B., & Chen, K. (2019). Development and characterization of bilayer films based on pea starch/polylactic acid and use in the cherry tomatoes packaging. *Carbohydrate Polymers, 222*(15), 114912.

Zuo, Y., Chen, K., Li, P., He, X., Li, W., & Wu, Y. (2020). Effect of nano-SiO_2 on the compatibility interface and properties of polylactic acid-grafted-bamboofiber/polylactic acid composite. *International Journal of Biological Macromolecules, 157*, 177-186.

CRediT authorship contribution statement

Fei Xiang: Investigation, Methodology, Writing - original draft. **Yuting Xia**: Investigation, Validation. **Yan Wang**: Investigation, Validation. **Yixin Wang**: Investigation, Review. **Kao Wu**: Data curation, Software. **Xuewen Ni**: Project administration, Methodology, Conceptualization, Funding acquisition, Writing - review & editing.

Declaration of Competing Interest

The authors declare that they have no conflict of interest.